BIBLIOGRAPHIC INFORMATION SYSTEM

JOURNAL FULL TITLE: Journal of Biomedical Research & Environmental Sciences
ABBREVIATION (NLM): J Biomed Res Environ Sci **ISSN:** 2766-2276 **WEBSITE:** https://www.jelsciences.com

SCOPE & COVERAGE

- **Sections Covered:** 34 specialized sections spanning 143 topics across Medicine, Biology, Environmental Sciences, and General Science
- Ensures broad interdisciplinary visibility for high-impact research.

PUBLICATION FEATURES

- **Review Process:** Double-blind peer review ensuring transparency and quality
- **Time to Publication:** Rapid 21-day review-to-publication cycle
- **Frequency:** Published monthly
- **Plagiarism Screening:** All submissions checked with iThenticate

INDEXING & RECOGNITION

- **Indexed in:** Google Scholar, IndexCopernicus (**ICV 2022: 88.03**)
- **DOI:** Registered with CrossRef (**10.37871**) for long-term discoverability
- **Visibility:** Articles accessible worldwide across universities, research institutions, and libraries

OPEN ACCESS POLICY

- Fully Open Access journal under Creative Commons Attribution 4.0 License (CC BY 4.0)
- Free, unrestricted access to all articles globally

GLOBAL ENGAGEMENT

- **Research Reach:** Welcomes contributions worldwide
- **Managing Entity:** SciRes Literature LLC, USA
- **Language of Publication:** English

SUBMISSION DETAILS

- Manuscripts in Word (.doc/.docx) format accepted

SUBMISSION OPTIONS

- **Online:** https://www.jelsciences.com/submit-your-paper.php
- **Email:** support@jelsciences.com, support@jbresonline.com

HOME ABOUT ARCHIVE SUBMIT MANUSCRIPT APC

Vision: The Journal of Biomedical Research & Environmental Sciences (JBRES) is dedicated to advancing science and technology by providing a global platform for innovation, knowledge exchange, and collaboration. Our vision is to empower researchers and scientists worldwide, offering equal opportunities to share ideas, expand careers, and contribute to discoveries that shape a healthier, sustainable future for humanity.

JOURNAL OF BIOMEDICAL RESEARCH & ENVIRONMENTAL SCIENCES
issn: 2766-2276
SUBJECT AREA(S): CLINICAL CARDIOLOGY | CARDIOVASCULAR DISEASES | PATHOLOGY
DOI: 10.37871

RESEARCH ARTICLE

Down-Regulation of Ephrin-B1 in Left Ventricular Non-Compaction

Andrea Frustaci[1*], Antonio Russo M[2], Alessandro De Luca[3], Davide Scarselli[3], Maria Cecilia D Asdia [3] Aurora Polvani[4], Emanuela Frustaci[4], Manuel Belli[5,6], Luigi Sansone[5,6], Nicola Galea[7], Livia Marchitelli[7] and Romina Verardo[1]

[1]Cellular and Molecular Cardiology Lab, IRCCS L. Spallanzani, Rome,Italy
[2]IRCCS San Raffaele Pisana, Rome, Italy
[3]Medical Genetics Laboratory, Fondazione IRCCS Casa Sollievo della Sofferenza, San Giovanni Rotondo, Italy
[4]Technoscience, Parco Scientifico e Tecnologico Pontino, Latina, Italy
[5]Department of Human Sciences and Promotion of the Quality of Life, San Raffaele Roma Open University, Rome 00166, Italy
[6]Laboratory of Molecular and Cellular Pathology, IRCCS San Raffaele Roma, 00166 Rome, Italy
[7]Department of Clinical, Internal, Anesthesiology and Cardiovascular Sciences, Sapienza University of Rome, Italy

Abstract

Background: Left Ventricular Non-Compaction (LVNC) is a rare cardiomyopathy with incompletely understood pathophysiological mechanisms. Ephrin-B1 (Ep), a key protein of cardiomyocyte lateral junctions, may play a role in cell cohesion. This study is aimed to characterize structural alterations of lateral junctions, quantify Ep expression, and identify genetic variants associated with LVNC.

Methods: We conducted an observational study on 13 patients from 12 independent families diagnosed with LVNC using cardiac magnetic resonance and endomyocardial biopsy. Histological, ultrastructural, and molecular analyses, including Ep expression and whole exome sequencing, were performed. Myocardial PCR was obtained for viral agents screening.

Results: Cardiomyocyte disconnection at lateral junctions was observed in all cases, ranging up to complete cell separation, while intercalated discs were preserved. The resulting intramural channels were extensively devoid of endothelial layer with frequent over-imposition of thrombotic material. Ep expression was reduced by 64% compared with controls (6229 ± 3197 vs 21451 ± 5054 densitometric units; absolute difference −15222; $p < 0.001$). Lymphocytic myocarditis

***Corresponding author(s)**

Andrea Frustaci, Cellular and Molecular Cardiology Lab, IRCCS L. Spallanzani, Rome, Via Portuense, 00149, Rome, Italy
Tel: +39-065-517-0520
Email: biocard@inmi.it

DOI: 10.37871/jbres2296

Submitted: 20 April 2026

Accepted: 28 April 2026

Published: 29 April 2026

Keywords

- Molecular and cellular Rehabilitation
- Intramural channels
- Ephrin-B1
- Exome
- Left ventricular noncompaction

VOLUME: 7 ISSUE: 4 - APRIL, 2026

How to cite this article: Frustaci A, Russo AM, Luca AD, Scarselli D, Asdia MCD, Polvani A, Frustaci E, Belli M, Sansone L, Galea N, Marchitelli L, Verardo R. Down-Regulation of Ephrin-B1 in Left Ventricular Non-Compaction. J Biomed Res Environ Sci. 2026 Apr 29; 7(4): 15. Doi: 10.37872/jbres2296

was present in 6 of 13 patients (46%; approximate CI 19–75%). Cardiomyopathy-related genetic variants were identified in 8 of 13 patients (61.5%). The EPHA2 polymorphism rs3754334 was found in 11/13 patients (85%) compared with 28% in the European population. No viral genomes were detected at myocardial PCR.

Conclusions: LVNC is characterized by lateral cardiomyocyte disconnection and marked down-regulation of Ep. Intramural channels often lacks of endothelium and are side of thrombus formation. Virus-negative myocarditis coexists in 46% of cases. These findings may contribute to arrhythmias, thromboembolism, and heart failure.

- **What is already known on this topic?**

  LVNC is a rare cardiomyopathy with unclear pathogenesis and heterogeneous genetic background. The cellular basis of cardiomyocyte disorganization and the role of lateral junction proteins are poorly understood.

- **What this study adds?**

  LVNC is characterized by cardiomyocyte disconnection at lateral junctions with marked Ephrin-B1 down-regulation. A high prevalence of virus-negative myocarditis (46%) and cardiomyopathy-related variants, including EPHA2 polymorphism enrichment, was identified.

- **How this study might affect research, practice or policy?**

  These findings support assessing myocardial inflammation and junctional integrity in LVNC. They suggest potential benefit of immunosuppressive therapy in selected cases and provide new targets for diagnosis and treatment.

Introduction

Left Ventricular Noncompaction (LVNC) is a rare congenital cardiomyopathy which prevalence has been reported between 0.014 and 1.3% in the general population [1]. Its identification has been variously obtained as by echocardiographic parameters with the recognition of LV non-compaction/compaction ratio ≥ 2 [2], cardiac magnetic resonance imaging with LV non-compaction/compaction ratio> 2.3 [3] or LV angiography showing perfused intramural channels arising from the endocardium.

Few systematic pathologic studies analyzed the histologic and ultrastructural changes of human LVNC and their related clinical implications. Finally, no distinctive genetic mutations have been identified so far that can explain its molecular and morphological pathway. So that actually LVNC is still defined an unclassified cardiomyopathy.

Ep is a structural protein of recent identification [4] recognized as a specific component of the lateral membrane of cardiomyocytes that appears to be essential for the stability of cell cohesion and maintenance of cardiac architecture. It is not expressed in other intracellular components of myocytes although it appears to compromise, in a KO mice model, the integrity of the intercalated disk as well as of the sarcomere apparatus, and finally the function of conduction tissue [5].

In the following report we evaluate in left ventricular endomyocardial biopsies from patients with LVNC, histologic and ultrastructural changes, thrombogenic predisposition of the disease and expression of Ep which can be involved in the lateral separation and then complete disconnection of

cardiomyocytes. These descriptions can explain clinical manifestations and outcome of LVNC.

We finally analyze the entire exome from different families affected by LVNC to hopefully find out common gene mutations.

Methods

The study included 13 patients (4 females and 9 males) from 12 independent families, diagnosed with Left Ventricular Non-Compaction (LVNC), consisting of 8 males and 5 females, with a mean age of 48 ± 12.8 years. Diagnosis was made by Left Ventricular Endomyocardial Biopsy (LVEMB), supported by cardiac magnetic resonance (non-compaction/compaction ratio > 2.3) and left ventricular angiography (showing intramural channels arising from the endocardium). Among them, 6 patients had reduced left ventricular ejection fraction (LVEF < 50%).

In all patients, cardiac investigations included non-invasive (ECG, Holter, 2D-echo, CMR) and invasive (Coronary, left ventricular angiography and endomyocardial biopsy) studies after written informed consent. Biopsy samples were processed for histology and electron microscopy. The assessment of Ephrin B1 (Ep) was obtained through immunofluorescence and protein isolation for Western Blot analysis.

The study complies with the Declaration of Helsinki, the locally appointed ethics committee approved the research protocol and informed consent was obtained from all subjects.

Cardiac Magnetic Resonance (CMR)

After obtaining written informed consent, Cardiac Magnetic Resonance imaging (CMR) was performed using a 1.5 T scanner (Magnetom Avanto, Siemens Medical Systems, Erlangen, Germany) equipped with body and phased-array coils. A single dose of gadoteric acid (Claricyclic, GE Healthcare, Chicago, Illinois, USA) at 0.25 ml/kg was injected intravenously at a flow rate of 2 ml/s.

The imaging protocol included:

- cine steady-state free precession (cine-SSFP) sequences acquired during breath-holds in short-axis views (10–12 slices from base to apex) and 2-chamber and 4-chamber planes.
- T2-weighted breath-hold black-blood short tau inversion recovery (STIR) sequences in short-axis views (8–10 slices from base to apex) and 2- and 4-chamber planes.
- Phase-sensitive inversion recovery gradient echo (PSIR-GRE) sequence was used 10–15 minutes after gadolinium injection for late gadolinium enhancement (LGE) imaging.
- T1 mapping performed using the Modified Look-Locker Inversion Recovery (MOLLI) sequence with a 5(3)3 scheme. MOLLI acquisitions included three axial slices (basal, mid-ventricular, and apical planes), both pre-contrast and 15 minutes post-contrast.
- T2 mapping was obtained using a T2-3pt GRE sequence in short-axis views covering basal, mid-ventricular, and apical planes.

Image analysis

- Two radiologists with 7 years and over 20 years of experience in Cardiovascular Imaging, respectively, performed image analysis using dedicated software (Cvi42, Calgary, Canada).
- The global and regional ventricular function were assessed using cine-SSFP.
- Endocardial and epicardial contours were semiautomatically traced on short axis planes at end-diastolic and end-systolic phases, to determine left ventricular volumes and ejection fraction (EF).

- The following validated CMR diagnostic criteria for left ventricular non-compaction (LVNC) were evaluated in all patients and volunteers: a non-compacted (NC) to compacted (C) myocardium diameter ratio > 2.3 in end-diastole [3], NC constituting >20% of left ventricular (LV) mass [6] and NC indexed mass >15 g/m^2 [7].
- Measurements of NC and C myocardial thickness, used to calculate the NC: C ratio, were performed on end-diastolic short-axis cine images, ensuring the myocardium was orthogonal to the measurement plane.
- To evaluate NC mass, a previously described [6,7], semi-automated, threshold-based technique was used to delineate the end-diastolic endocardial border of the NC myocardium, along with standard epicardial contours, to calculate the "global myocardial mass." The NC mass was determined by subtracting the compacted (C) myocardial mass (calculated using standard endocardial and epicardial contours) and the papillary muscle mass from the global myocardial mass.
- LGE and STIR images was considered positive according to current standards.
- The 95th percentile values in the control group served as thresholds for abnormalities, with T1 ranging from 970 to 1027 ms, T2 and ECV being less than 49.9 ms and 29.5%, respectively.

Invasive and endomyocardial biopsy studies

Cardiac catheterization with left ventricular and coronary angiography was obtained in all patients. Endomyocardial biopsy (four to 8 samples each patient) was performed in the septal-apical region of left ventricle.

Histology and electron microscopy

For histological analysis the endomyocardial samples were fixed in 10% buffered formalin and paraffin embedded. Five-micron thick sections were stained with hematoxylin & eosin and Masson trichrome.

For electron microscopy studies, additional samples were fixed in 2% glutaraldehyde in a 0.1 M phosphate buffer, at pH 7.3, post-fixed in osmium tetroxide and processed following a standard protocol for embedding in epon resin. Ultrathin sections were stained with uranyl acetate substitute and lead hydroxide. Ultrastructural analysis and pictures were performed with a Jeol 1400 plus TEM.

Molecular study

The molecular study was performed in the all patients with Real Time PCR for the most common cardiotropic viruses (Adenovirus, Enterovirus, Influenza A and B virus, Epstein Barr virus, Parvovirus B19, Hepatitis C virus, Cytomegalovirus, Human Herpes virus 6, Herpes Simplex type 1 and 2) for the possible identification of viral genomes.

Assessment of Ephrin B1 in the myocardial tissue of LVNC patients

We determined the expression of Ep in frozen myocardial tissue. Results were compared with values from surgical control unloaded myocardium (papillary muscle of patients with mitral stenosis undergoing valve replacement).

Immunofluorescence and immunohistochemistry studies

We performed immunofluorescence staining using an anti-Mouse Ephrin-B1 antibody (R&D Systems, AF473, Minneapolis, MN, USA) diluted 1:10. Samples were incubated overnight at 4 °C to ensure optimal binding, followed by washing steps and incubation with fluorescent secondary antibodies to visualize Ep expression.

For immunohistochemistry, we used a rabbit anti-von Willebrand Factor (vWF) antibody (Sigma-Aldrich Corporation, F3520, Missouri USA), diluted 1: 20 (Sigma-Aldrich, F3520) to detect endothelialization in the intramyocardial channels.

Protein isolation and western blot

Heart tissue samples were treated as previously described. The expression of Ep was visualized by using Mouse Ephrin-B1, 1:100 overnight (R &D SYSTEM, AF473, Minneapolis MN 55413) molecular weight 45-50 kDa, followed by HRP-coniugated Anti-Goat IgG secondary antibody, 1:5000(Jackson ImmunoResearch Laboratories,Inc) . Anti-α-sarcomeric actin antibody (1:500, Sigma-Aldrich), molecular weight 43 kDa, was used for normalization. Signal was visualized using enhanced chemiluminescence (ECL Clarity Bio-Rad). The purity as well as equal loading (40γ) of the protein was determined by Nanodrop One (Thermofisher). To normalize target protein expression, the band intensity of each sample is determined by densitometry with Image J software. Next, the intensity of the target protein is divided by the intensity of the loading control protein. This calculation adjusts the expression of the protein of interest to a common scale and reduces the impact of sample-to-sample variation. Relative target protein expression can then be compared across all lanes to assess changes in target protein expression across samples. Digital images of the resulting bands were quantified by the Image Lab software package (Bio-Rad Laboratories, Munchen, Germany) and expressed as arbitrary densitometric units.

Gene studies

Molecular analysis

- **DNA Extraction:** Genomic DNA (gDNA) was extracted from peripheral blood using a manual kit (Macherey-Nagel, Düren, Germany), following the manufacturer's instructions. DNA concentration was measured with a Qubit™ fluorometer (Invitrogen, Carlsbad, CA, USA), and purity was assessed using a NanoDrop 1000 spectrophotometer (Thermo Scientific, Waltham, MA, USA). Acceptable purity thresholds were defined as 260/280 ≈ 1.8–2.0 and 230/280 ≈ 1.8–2.0.

- **Parallel sequencing:** Whole exome sequencing (WES) was outsourced to Aurogene (Rome, Italy). WES analysis was performed at a target coverage of 200×, starting from ≥20 µl of high-quality gDNA at a concentration of ≥25 ng/µl. Libraries were prepared using the xGen DNA Library Prep EZ Kit and the xGen Exome Hyb Panel v2 Kit with unique dual indexes (Integrated DNA Technologies, Coralville, IA, USA). The workflow included sample quality control, library preparation, and final quality control. Sequencing was carried out on an Illumina NovaSeq platform (Illumina, San Diego, CA, USA) with a 2 × 150 bp paired-end run, yielding ≥18 Gb per sample, Q30 ≥85%, and a target coverage of 200×. The bioinformatics pipeline provided by the service included demultiplexing, filtering, and trimming. Raw data were delivered as FASTQ files with optional quality reports.

Variant annotation, filtering, and classification: Sequencing reads were aligned to the human reference genome (GRCh38/hg38) using Bowtie 2 (v2.3.0). BAM files were sorted with SAMtools (v1.3.2), and PCR duplicates were removed with the MarkDuplicates tool from the Picard suite (v2.9.0). Local realignment and base quality score recalibration were performed with the Genome Analysis Toolkit (GATK v4.0). Reads with mapping quality <20 were excluded. Variant calling was carried out using GATK HaplotypeCaller. Variants were annotated with ANNOVAR and filtered to exclude common polymorphisms with a minor allele frequency (MAF) >1% in dbSNP (https://www.ncbi.nlm.nih.gov/projects/SNP/), GO-ESP (https://esp.gs.washington.edu/drupal/), and gnomAD

(http://gnomad.broadinstitute.org/) [8-14]. Importantly, this frequency-based filtering was not applied to *Ephrin*-related genes, which were retained for downstream analysis regardless of MAF.

Pathogenicity of candidate variants was assessed using multiple *in silico* prediction tools: MutationTaster, PolyPhen-2, MutationAssessor, PROVEAN, SIFT, and Combined Annotation Dependent Depletion (CADD v1.3). Potential splice-altering variants were evaluated with SpliceSiteFinder-like, MaxEntScan, NNSPLICE, and Human Splicing Finder (all integrated in the Alamut Software suite, Interactive Biosoftware, Rouen, France), as well as with the dbscSNV algorithm incorporated in VarSome (https://varsome.com/](https://varsome.com/), which provides "ADA" and "RF" splice prediction scores.

Variant classification was performed according to the standards and guidelines of the American College of Medical Genetics and Genomics and the Association for Molecular Pathology (ACMG-AMP) for the interpretation of sequence variants [15].

Results

CMR data

- CMR data are depicted in table 1.
- Nearly half of the patients (41%) presented impaired LVEF (mean value 50 ± 13%) and 25% of patients showed increased left ventricle end-diastolic volume (LVEDV)/BSA volume (mean value 102 ± 51%).
- All patients met at least one validated CMR diagnostic criterion for LVNC. The mean value of NC indexed mass was 24 ± 15 g/m^2, and the mean NC/LV mass percentage was 25 ± 8 % (Figure 1).
- Myocardial edema was found on T2 weighted images in 6/13 patients, as depicted in figure 2.

Invasive cardiac studies

LV angiography documented in all cases the presence of large intramural channels arising from the endocardial surface and running into the myocardium up to the sub-epicardial layer. In 6 out of 13 patients a reduced cardiac contractility (LVEF< 50%) was registered. No complications associated with cardiac catherization, LV angiography and endomyocardial biopsy were reported.

Histology and EM

Regularly arranged, mildly to moderately hypertrophied myocytes were observed. Cardiomyocytes showing various degree of disconnection up to total cell separation were diffusely documented (Figure 3, panel a).

In particular cell detachment occurred systematically at myocyte lateral junction (Figure 3, panel b).

Importantly, the surface of infoldings is lacking of endocardial layer and then cellular and plasma blood constituents appear in direct contact with cardiomyocyte plasma membrane (Figure 4).

This is confirmed by IHC for vWF a specific endothelial biomarker which is absent in major part of the surface of intramural lacunae (Figure 5).

Notably, intercalated disc structure of the cardiomyocytes is constantly intact including

Table 1: CMR features.

CMR Features	
LVEDV/BSA (mL/m^2), mean ± SD	101.8 ± 51.1
LVESV/BSA (mL/m^2), mean ± SD	53.4 ± 39.6
LVEF (%), mean ± SD	49.8 ± 12.9
Indexed NC mass	24.2 ± 15.4
NC/LV mass, %	25 ± 7.9
Native T1 global (ms), mean ± SD	1065.8 ± 54.2
T2 global (ms), mean ± SD	51 ± 3.4
Edema on T2w images, n (%)	12 (70%)
LGE presence, n (%)	8 (47%)

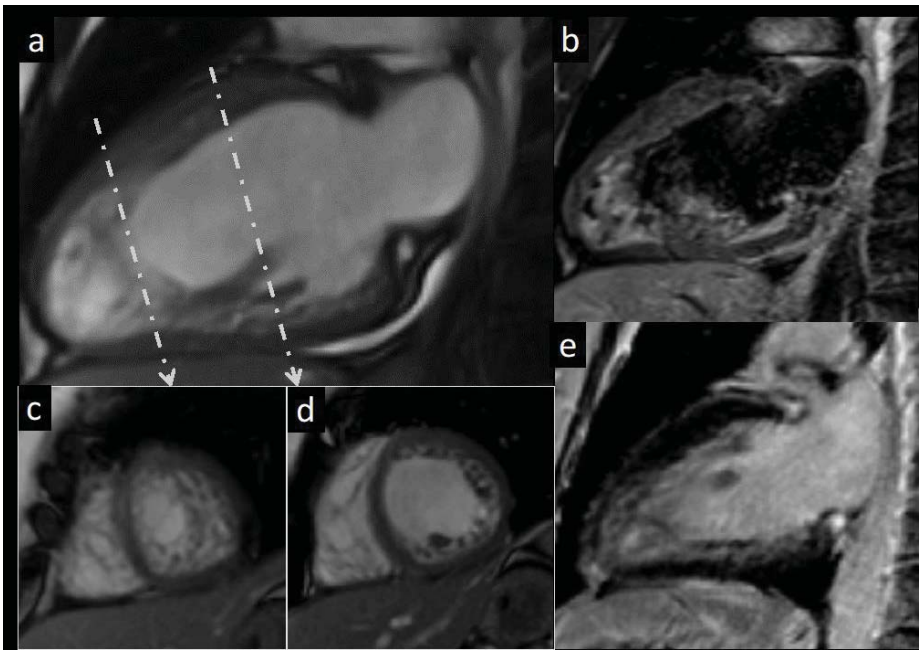

Figure 1 CMR images of a 28-y.o. woman which meet all CMR diagnostic criteria for LVNC (NC/C ratio = 3, NC/LV mass = 21, indexed NC mass = 22 g/m^2) on 4ch (a) and short axis (c,d) cineMR images. No signs of edema or fibrosis was found at conventional STIR (b) and LGE (e) images. CMR: Cardiac Magnetic Resonance; LVNC: Left Ventricle Non-Compaction; NC: Non Compacted; C: Compacted; cineMR: cine Magnetic Resonance; STIR: short-tau Inversion Recovery; LGE: Late Gadolinium Enhancement.

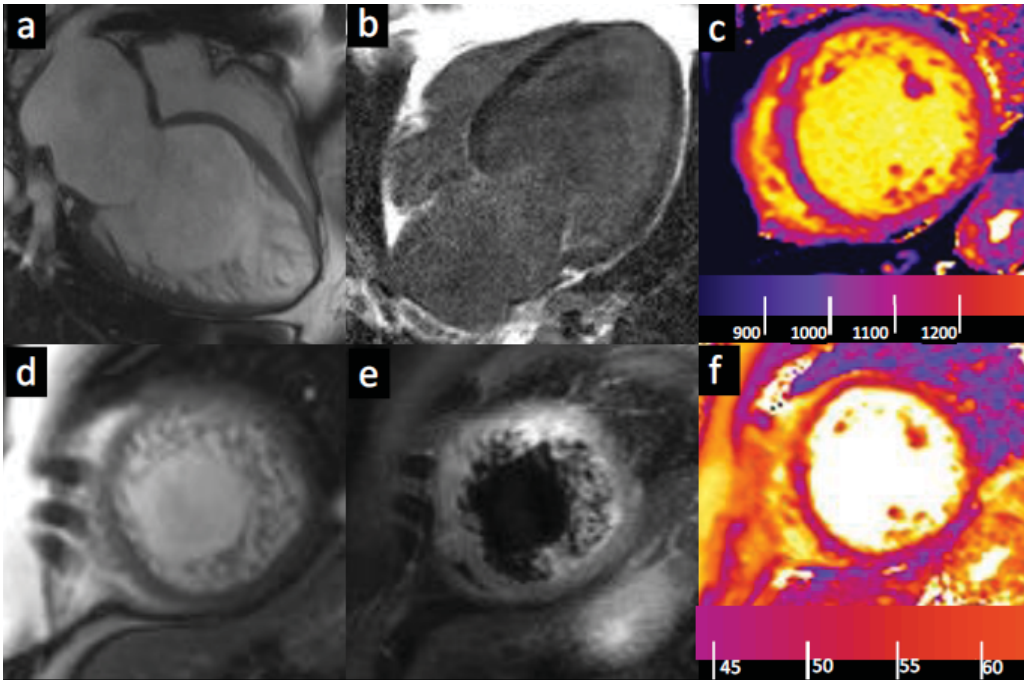

Figure 2 CMR images of a 50-y.o. man which meet all CMR diagnostic criteria for LVNC (NC/C ratio = 3.5, NC/LV mass = 38%, indexed NC mass = 74 g/m^2) on 4ch (a) and short axis (d) cineMR images. Both conventional (b and e) and mapping (c and f) shows signs of edema, expressed as hyperintensity on STIR images (e) and increase on T2 values (f) and diffuse fibrosis, expressed as nuanced hyperintensity on LGE images (b) and increase in nT1 values (c).CMR: Cardiac Magnetic Resonance; LVNC: Left Ventricle Non-Compaction; NC: Non-Compacted; C: Compacted; cineMR: cine Magnetic Resonance; STIR: short-tau Inversion Recovery; nT1: native T1; LGE: Late Gadolinium Enhancement.

the morphology of various junctional complexes (Figure 3 and figure 4). This suggests that genetic alterations of junctional proteins evidenced in some our patients (see table 2) are not involved in intercalated disc disorganization.

Evidences of thrombogenesis in the trabecular lacunae

Intramural infoldings or lacunae are part of extracellular space of the cardiac chambers and then contain polymorphic erythrocytes, leukocytes, platelets, cell debris from cardiomyocytes and intact small vessels or capillaries. Platelets may be in normal resting state (unchanged shape with some granules) (Figure 6a) or may form agglutinate in the lumen of some intact vessels (Figure 6). More frequently, in the lacunar space, platelets show an early activation with shape change and pseudopod formation (Figure 6b), forming small early aggregates (Figure 6c) and mature thrombi (Figure 6d).

Overlapping myocarditis

In a subset of our patients (6/13) inflammatory mononuclear infiltrates associated to necrosis of the adjacent myocytes suggesting a virus-negative overlapping myocarditis were present in the trabecular myocardium (Figure 7).

Molecular study

All patients were negative for the presence of viral genomes.

Gene studies

Molecular analysis: Mutational analysis was performed on 13 individuals from 12 independent families using targeted next-generation sequencing of a panel comprising 110 candidate genes implicated in cardiomyopathies

Table 2: Genetic variants identified in the study cohort. Variants detected in 13 independent probands by WES analysis. For each subject, the following information is provided: laboratory code, sex, gene (*italicized*), reference sequence (RefSeq), genomic and protein alterations (HGVS nomenclature), variant type, protein function, ACMG–AMP criteria and classification, and genotype at the rs3754334 (*EPHA2*) and rs9881589 (*EPHB3*) polymorphisms.

Lab code	Sex	Gene[A]	Nucleotide change	Protein alteration	Variant type	Protein function	ACMG/AMP criteria	ACMG/AMP classification	*EPHA2*[B,C]
1	M	Negative							Homozygote
2	M	*LMNA*	c.1367A>G	p.Asn456Ser	Missense	Structural/contractive (sarcomere,cytoskeleton)	PM1, PM5, PP3,PP5,PM2	P	Homozygote
3	M	*ACTC1*	c.62C>T	p.Ala21Val	Missense	Structural/contractive (sarcomere,cytoskeleton)	PP3,PM2,PP2,PP5	LP	Homozygote
4	M	*ACTC1*	c.62C>T	p.Ala21Val	Missense	Structural/contractive (sarcomere,cytoskeleton)	PP3,PM2,PP2,PP5	LP	Homozygote
5	M	*ACTC1*	c.1094A>G	p.Asp365Gly	Missense	Structural/contractive (sarcomere,cytoskeleton)	PP3,PM2,PP2	LP	Wild-type
6	M	*SLC22A5*	c.34G>A	p.Gly12Ser	Missense	Metabolic/transport	PP5,PM1,PM5,PM2	LP	Heterozygote
7	F	*MYH6*	c.253G>A	p.Asp85Asn	Missense	Structural/contractive (sarcomere,cytoskeleton)	PM2	VUS	Heterozygote
		DSC2	c.1069C>T	p.Arg357Cys	Missense	Cell adhesion (desmosome)	PM2,BP1,BP4	VUS	
8	M	*VARS*	c.1258G>A	p.Ala420Thr	Missense	Translation machinery	PP5,PM2	VUS	Heterozygote
9	M	Negative							Heterozygote
10	M	Negative							Heterozygote
11	F	Negative							Heterozygote
12	F	Negative							Wild-type
13	F	*PTPN11*	c.1415C>T	p.Thr472Met	Missense	Signaling/Pathway regulation	PS3,PP3,PP5,PM1,PM5,PM2	P	Heterozygote

M, missense; P, pathogenic, LP, likely pathogenic, VUS, variant of uncertain significance, LB, likely benign.
[A]RefSeqs: *LMNA*, NM_170707.4; *ACTC1*, NM_005159.5; *SLC22A5*, NM_001308122.2; *MYH6*, NM_002471.4; *DSC2*, NM_024422.6; *VARS*, NM_001167734.2; *PTPN11*, NM_001330437.2.
[B]*EPHA2* genotypes: homozygote (A/A), heterozygote (G/A), wyld-type (G/G).
[C]dbSNP code: rs375433

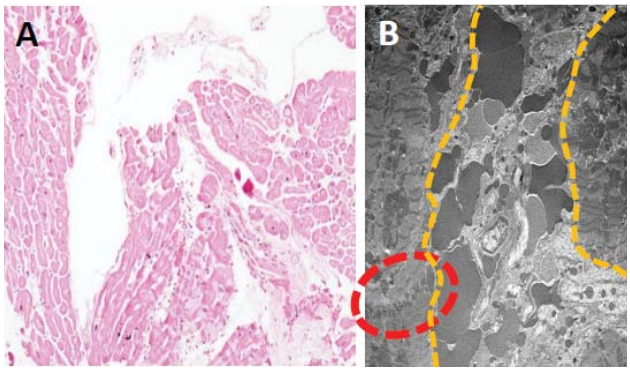

Figure 3 Panel A - Histological section in H&E (200 X) of a LV endomyocardial biopsy from a patient affected by LVNC showing diffuse cardiomyocytes' disconnection with formation of large intramural channels. Panel B - TEM microscopy of a LV endomyocardial biopsy from a patient with LVNC showing lateral detachment of cardiomyocytes which surface is completely unendotheliolized.

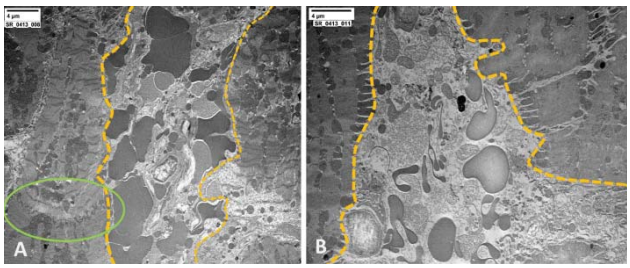

Figure 4 TEM of a LV endomyocardial biopsy from a patient with LVNC.
Panel A – Large lacuna (extracellular space) of the trabecular myocardium not covered by endothelium. Lacuna contains polymorphic and clumped erythrocytes, cell debris from cardiomyocytes and red cells. The ellipse indicates a well-structured intercalated disc. Myo = myocardium; L = lumen of the vessel; RC = red cell. The bar represents 4 mm.
Panel B – Large lacuna of the trabecular myocardium lacking the endothelial lining. Polymorphic red cells, cell debris of different origin and an intact capillary (arrows) are present in the myocardial extracellular space. Myo = myocardium; L = lumen of the vessel; RC = red cell. The bar represents 4 µm.

(Table 2). WES analysis identified genetic variants associated with cardiomyopathy-related phenotypes were identified in 8 of the 13 subjects (61.5%). Among these, 6 probands carried variants classified as *pathogenic* or *likely pathogenic* according to ACMG–AMP guidelines, while 2 carried *variants of uncertain significance* (VUS) . One proband (#7) harbored two independent variants, both classified as VUS according to ACMG–AMP criteria [15].

Heterozygous variants in sarcomeric protein genes were identified in five probands from four families. Specifically, three probands from two unrelated families carried missense variants in the *ACTC1* gene. One family (cases #3 and #4, previously described by Frustaci, et al. [16] harbored the same missense variant, p. Ala21Val. Another missense variant was detected in *MYH6* (classified as VUS); this proband (#7) also carried an additional VUS in the cell adhesion gene *DSC2*.

A pathogenic missense variant was identified in the laminopathy gene *LMNA*, while another proband carried a likely pathogenic missense variant in *SLC22A5*, a gene associated with primary carnitine deficiency—an autosomal recessive disorder—although no second allele was detected. Another proband harbored a VUS in the *VARS* gene, which encodes valyl-tRNA synthetase, an essential enzyme in protein translation. One cardiomyopathy case was

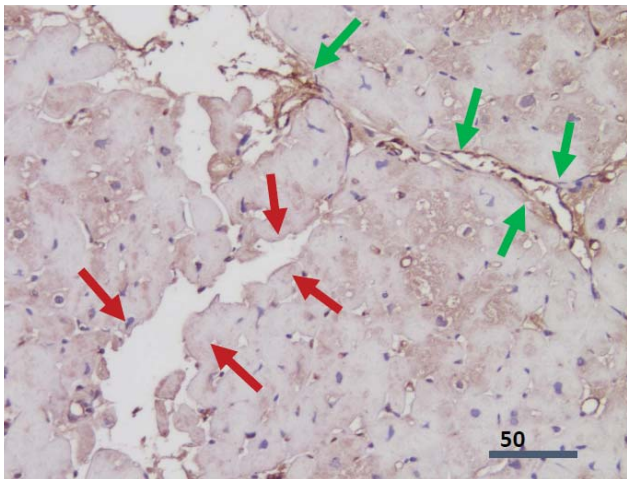

Figure 5 IHC of LV endomyocardial biopsy from a patient with LVNC, treated with anti-vWF Ab.
Von Willebrand Factor is a highly specific biomarker of endothelial cells, which in this sample is absent, in large lacunae (red arrows), while can be present in smaller extracellular spaces (green arrows). The bar represents 50 µm.

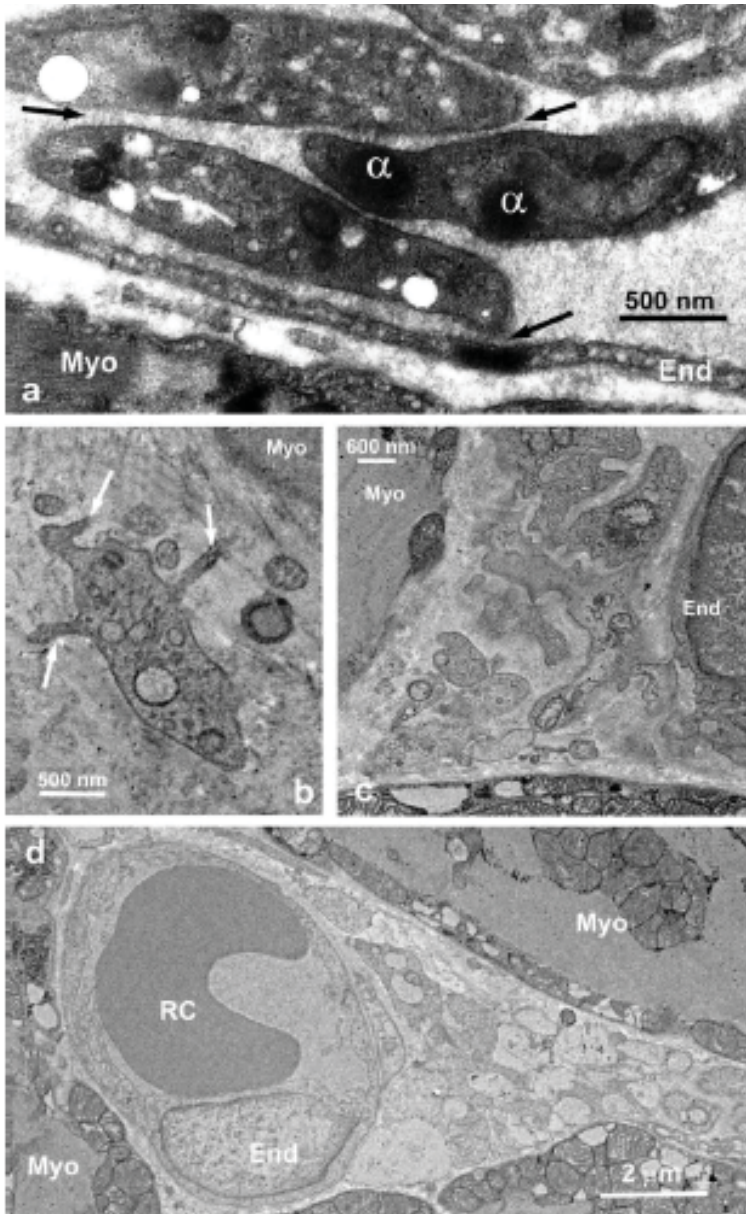

Figure 6 TEM - Ultrastructural changes of platelet activation and thrombus formation in lacunae of trabecular myocardium.
Panel A – Platelet agglutination. Groups of disc-shaped platelets can be attached to the endothelium in the lumen of vessels of trabecular myocardium close to the spaces of non-compacted myocardium. Platelets appear in resting state with unchanged shape and no signs of pseudopod emission and of granule secretion. However, platelets strictly interact with endothelium and/or each other, forming tight electron-dense junctions (20-30 nm wide; see arrows). Myo = myocardium; End = endothelium; a = a-granules. The bar represents 500 nm.
Panel B - Platelet shape change. Platelets showing typical early shape change with pseudopod emission and release of granules. They be frequently observed in the extracellular spaces of trabecular myocardium, with any relation with endothelial or other cells. Myo = myocardium. The bar represents 500 nm.
Panel C - Early small platelet aggregate in the extracellular space of trabecular myocardium. Platelets have drastically changed their shape and secreted most of granules. Platelet-to-platelet junction are still large (30-100 nm). Myo = myocardium; End = endothelium. The bar represents 600 nm.
Panel D – Late platelet aggregate in the extracellular space of the trabecular myocardium. Platelets show the typical structure seen in the advanced irreversible aggregate/thrombus: platelets are closely interacting (junctions of 20-25 nm), apparently completely empty of their granules and organelles with a swollen cytosol. The aggregate appears to interact with external wall of the capillary (End) and with the surface of well-preserved cardiomyocytes (Myo). RC = Red cell. The bar represents 2 microns.

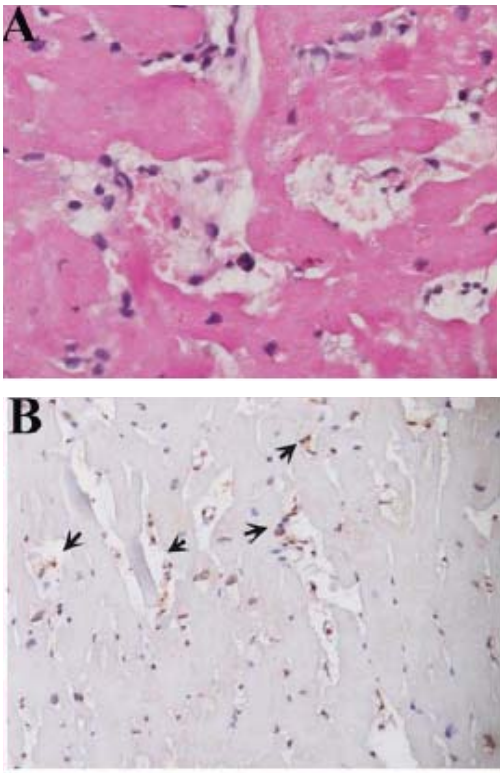

Figure 7 Overlapping virus-negative myocarditis in LVNC. Panel A - Ematoxylin-Eosin staining showing lymphocytic inflammatory infiltrates in channelled myocardial tissue associated with necrosis of adjacent myocytes. Panel B - CD45Ro staining identifying T lymphocytes.

associated with Noonan syndrome, caused by a well-established pathogenic variant in *PTPN11* [17]. No relevant variants were detected in five probands in the investigated genes.

Because immunohistochemical analyses showed reduced ephrin protein abundance in these probands, we further investigated this phenotype focusing on *ephrin*-encoding genes and their interactome. No rare or pathogenic variants were identified; therefore, the analysis was extended to polymorphisms within these genes. One polymorphism was observed at significantly higher frequencies in the cohort compared with European population data. In particular, the c.2874C>T (p.Ile958=, rs3754334) in the *EPHA2* gene, encoding ephrin type-A receptor 2, was detected in our cohort at a frequency of (0.54), compared with 0.28 in Europeans (non-Finnish) (p = 0.003711).

Western blot: Western blot analysis revealed that the expression of Ep in heart tissue was reduced by approximately 3.4-fold (64%) (Figure 8) in the samples compared to controls (6229 ± 3197 *vs.* 21451 ± 5054 arbitrary densitometric units). The difference was statistically significant ($p < 0.001$). Band intensities were normalized to α-sarcomeric actin, used as the loading control. Quantification was performed using Image Lab and ImageJ software. Control samples consisted of surgical myocardial biopsies (papillary muscle) obtained from patients undergoing cardiac surgery for mitral stenosis, with normal left ventricular volume and function.

Immunofluorescence studies: Immunofluorescence for Ep revealed a remarkable down-regulation in Left Ventricular (LV) biopsies from subjects with Left Ventricular Non-Compaction (LVNC) compared to normal controls. The fluorescent signal intensity was significantly reduced in the pathological samples, indicating decreased expression of Ep in LVNC tissue. This finding suggests a potential involvement of Ep in the altered molecular mechanisms associated with LVNC.

Statistical analysis

Statistical analysis was performed using GraphPad Prism software, version 5.02 (GraphPad Software Inc., San Diego, CA, USA). Continuous variables are expressed as mean ± standard deviation (SD), while categorical variables are presented as counts and percentages. Comparisons between groups were performed using the Mann–Whitney U test, as data distribution was not assumed to be normal given the small sample size. All tests were two-tailed. A $p\text{-}value < 0.05$ was considered statistically significant.

Discussion

Our study, analyzing left ventricular endomyocardial biopsies from 13 unrelated

patients with LVNC, documents a progressive cardiomyocyte disconnection toward a complete cell separation. Interestingly, cardiomyocyte detachment occurs, on electron microscopy observation, at lateral cell junction while the intercalated disks appear structurally preserved. Lateral junctions are essential components of the myocardial tissues since they confer cell to cell essential mechanical and electrical interactions. Their progressive reduction appears very likely implicated in the generation of cardiac arrhythmias, causing sometimes sudden death as well as of the impairment of left ventricular function and the evolution toward a dilated cardiomyopathy. The major structural component of lateral junctions is represented by Ep that results remarkably reduced to 3.4-fold lower than controls indicating the cause of myocyte disconnection.

The surface of intramural channels appears partially or totally unendotheliolized (Figure 3) and show platelet activation (Figure 6-panel A) and thrombi formation (Figure 6-panel D) explaining the systemic thromboembolism that affects this entity requiring the introduction of anticoagulants in the treatment of the disease. It remains to consider when to introduce anticoagulation: if when the LV dimensions and contractility are still normal or whether waiting for LV dilatation and dysfunction.

Overlapping virus-negative lymphocytic myocarditis was observed in 46% of the cases with LVNC. Among the possible causes an auto-reactive response to cell necrosis and to segregated antigens like myosin should be taken into consideration. This relatively high incidence of myocardial inflammation suggests it may concur to the manifestation and progression of the disease as in terms of cardiac arrhythmias as contributing to cardiac dilatation and dysfunction.

This observation may influence the treatment of the disease considering the potential benefit of immunosuppressive therapy (TIMIC 1 e 2) in virus-negative myocarditis that has been documented in 88% of treated patients (TIMIC 1), with maintenance of cardiac improvement in 94% of cases at 20 year follow-up (TIMIC 2) [18,19]; The possible presence of inflammation in LVCN should be then carefully evaluated by non-invasive (CMR) and possibly invasive procedures particularly in complex and severe cases.

Molecular analyses

Mutational analysis was performed on 13 individuals from 12 independent families using targeted next-generation sequencing of a panel comprising 110 candidate genes implicated in cardiomyopathies. WES analysis identified genetic variants associated with cardiomyopathy-related phenotypes were identified in 8 of the 13 subjects (61.5%). Among these, 6 probands carried variants classified as pathogenic or likely pathogenic according to ACMG–AMP guidelines, while 2 carried variants of uncertain significance (VUS) (Table 2). One proband (#7) harbored two independent variants, both classified as VUS according to ACMG–AMP criteria [15].

Heterozygous variants in sarcomeric protein genes were identified in five probands from four families. Specifically, three probands from two unrelated families carried missense variants in the ACTC1 gene. One family (cases #3 and #4, previously described by Frustaci, et al. [16] harbored the same missense variant, p.Ala21Val. Another missense variant was detected in MYH6 (classified as VUS); this proband (#7) also carried an additional VUS in the cell adhesion gene DSC2.

A pathogenic missense variant was identified in the laminopathy gene LMNA, while another proband carried a likely pathogenic missense variant in SLC22A5, a gene associated with primary carnitine deficiency—an autosomal recessive disorder—although no second allele

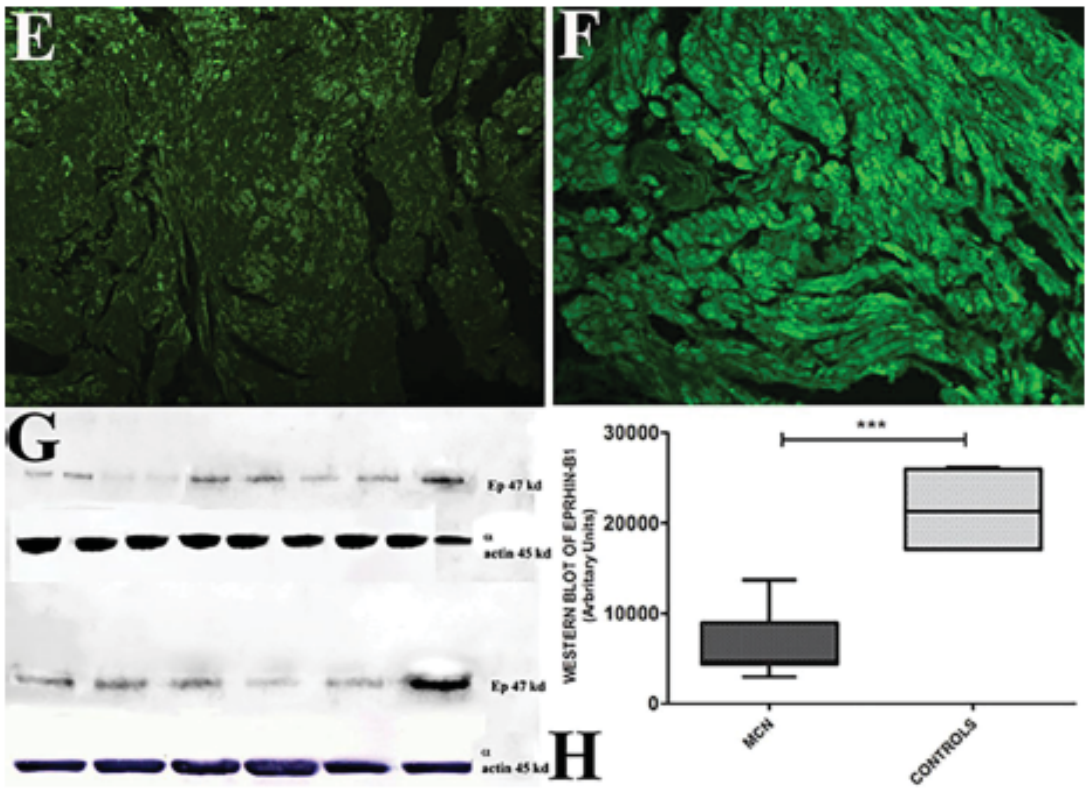

Figure 8 Immunofluorescence and Western blot analysis showing Ep reduction in LVNC.
Panels E-F - Immunofluorescence for Ep demonstrating its remarkable down-regulation in a LV biopsy from a LVNC subject (panel E) compared with normal control (panel F).
Panels G-H - Western blot quantification of Ep in the myocardium of 13 patients with LVNC (panel G) indicating a 3.4-fold reduction of Ep expression in LVNC pts vs normal controls (panel H) Alpha-sarcomeric actin (45 Kd) was used as control.

was detected. Another proband harbored a VUS in the VARS gene, which encodes valyl-tRNA synthetase, an essential enzyme in protein translation. One cardiomyopathy case was associated with Noonan syndrome, caused by a well-established pathogenic variant in PTPN11 [17]. No relevant variants were detected in five probands in the investigated genes.

Because immunohistochemical analyses showed reduced ephrin protein abundance in these probands, we further investigated this phenotype focusing on ephrin-encoding genes and their interactome. No rare or pathogenic variants were identified; therefore, the analysis was extended to polymorphisms within these genes. One polymorphism was observed at significantly higher frequencies in the cohort compared with European population data. In particular, the c.2874C>T (p. Ile958=, rs3754334) in the EPHA2 gene, encoding ephrin type-A receptor 2, was detected in our cohort at a frequency of (0.54), compared with 0.28 in Europeans (non-Finnish) (p = 0.003711).

Limitations of the study

This study has several limitations, including the small sample size, potential selection bias due to inclusion of biopsy-proven cases, and limited generalizability. Additionally, the observational design precludes causal inference

Clinical Implications and Future Directions

These findings suggest that LVNC pathogenesis involves both structural and inflammatory mechanisms. Future studies should investigate targeted therapies addressing myocardial inflammation and cell adhesion

pathways. Larger multicenter studies are needed to validate these observations.

Conclusion

LVNC is associated with lateral disconnection of cardiomyocytes and down- regulation of Ep. Overlapping virus-negative myocarditis is detectable in up to 46% of cases.

Acknowledgements

Funding

The study has been supported by project CARDIOMOMO, IRCCS L Spallanzani, and partially by Italian Health Ministry (IRCCS San Raffaele Roma–Ricerca Corrente #2021/1).

Institutional review board statement

The study was conducted in accordance with the Declaration of Helsinki, and approved by the locally appointed ethics committee (opinion number 6/2019 and 2016-003014-28 (FARM12JCXN) and informed consent was obtained from all subjects.

Informed consent statement

Informed consent was obtained from all subjects involved in the study.

Data availability statement

The datasets used and analyzed during the current study are avail-able from the corresponding author upon reasonable request.

Conflicts of interest

The authors declare that they have no competing interests.

References

1. Nunez-Gil IJ, Feltes-Guzman G. Left ventricular noncompaction. E J Cardiol Pract. 2012;10(31).
2. Jenni R, Oechslin E, Schneider J, Attenhofer Jost C, Kaufmann PA. Echocardiographic and pathoanatomical characteristics of isolated left ventricular non-compaction: a step towards classification as a distinct cardiomyopathy. Heart. 2001;86(6):666-671. doi:10.1136/heart.86.6.666
3. Petersen SE, Selvanayagam JB, Wiesmann F, Robson MD, Francis JM, Anderson RH, Watkins H, Neubauer S. Left ventricular non-compaction: insights from cardiovascular magnetic resonance imaging. J Am Coll Cardiol. 2005;46(1):101-105. doi:10.1016/j.jacc.2005.03.045
4. Genet G, Guilbeau-Frugier C, Honton B, et al. Ephrin-B1 is a novel specific component of the lateral membrane of the cardiomyocyte and is essential for the stability of cardiac tissue architecture cohesion. Circ Res. 2012;110(5):688-700. doi:10.1161/CIRCRESAHA.111.259093
5. Sachse FB, Moreno AP, Seemann G, Abildskov JA. A model of electrical conduction in cardiac tissue including fibroblasts. Ann Biomed Eng. 2009;37(5):874-889. doi:10.1007/s10439-009-9667-4
6. Jacquier A, Thuny F, Jop B, et al. Measurement of trabeculated left ventricular mass using cardiac magnetic resonance imaging in the diagnosis of left ventricular non-compaction. Eur Heart J. 2010;31:1098-1104. doi:10.1093/eurheartj/ehp595
7. Grothoff M, Pachowsky M, Hoffmann J, et al. Value of cardiovascular MR in diagnosing left ventricular non-compaction cardiomyopathy and in discriminating between other cardiomyopathies. Eur Radiol. 2012;22:2699-2707. doi:10.1007/s00330-012-2554-7
8. Schwarz JM, Rödelsperger C, Schuelke M, Seelow D. MutationTaster evaluates disease-causing potential of sequence alterations. Nat Methods. 2010;7:575-576.
9. Adzhubei I, Jordan DM, Sunyaev SR. Predicting functional effect of human missense mutations using PolyPhen-2. Curr Protoc Hum Genet. 2013;Chapter 7.20.
10. Reva B, Antipin Y, Sander C. Predicting the functional impact of protein mutations: application to cancer genomics. Nucleic Acids Res. 2011;39.
11. Choi Y, Sims GE, Murphy S, Miller JR, Chan AP. Predicting the functional effect of amino acid substitutions and indels. PLoS One. 2012;7.
12. Ng PC, Henikoff S. SIFT: predicting amino acid changes that affect protein function. Nucleic Acids Res. 2003;31:3812-3814.
13. Kircher M, Witten DM, Jain P, O'Roak BJ, Cooper GM, Shendure J. A general framework for estimating the relative pathogenicity of human genetic variants. Nat Genet. 2014;46:310-315.
14. Jian X, Boerwinkle E, Liu X. In silico prediction of splice-

altering single nucleotide variants in the human genome. Nucleic Acids Res. 2014;42:13534-13544.

15. Richards CS, Bale S, Bellissimo DB, et al. Standards and guidelines for the interpretation of sequence variants. Genet Med. 2008;10:294-300.

16. Frustaci A, De Luca A, Guida V, Biagini T, Mazza T, Gaudio C, Letizia C, Russo MA, Galea N, Chimenti C. Novel α-actin gene mutation p.(Ala21Val) causing familial hypertrophic cardiomyopathy, myocardial noncompaction, and transmural crypts. J Am Heart Assoc. 2018;7(4). doi:10.1161/JAHA.117.008068

17. Tartaglia M, et al. Mutations in PTPN11, encoding the protein tyrosine phosphatase SHP-2, cause Noonan syndrome. Nat Genet. 2001;29:465-468.

18. Chimenti C, Russo MA, Frustaci A. Immunosuppressive therapy in virus-negative inflammatory cardiomyopathy: 20-year follow-up of the TIMIC trial. Eur Heart J. 2022;43(36):3463-3473. doi:10.1093/eurheartj/ehac348

19. Frustaci A, Russo MA, Chimenti C. Randomized study on the efficacy of immunosuppressive therapy in patients with virus-negative inflammatory cardiomyopathy: the TIMIC study. Eur Heart J. 2009;30(16):1995-2002. doi:10.1093/eurheartj/ehp249.